Journal of Materials Chemistry A

PAPER

View Article Online
View Journal | View Issue

Cite this: J. Mater. Chem. A, 2016, 4, 18614

Influence of mobile ions on the electroluminescence characteristics of methylammonium lead iodide perovskite diodes†

Enrico Bandiello,[a] Jorge Ávila,[a] Lidón Gil-Escrig,[a] Eelco Tekelenburg,[b] Michele Sessolo*[a] and Henk J. Bolink[a]

Received 10th August 2016
Accepted 1st November 2016

DOI: 10.1039/c6ta06854e

www.rsc.org/MaterialsA

In this work, we study the effect of voltage bias on the optoelectronic behavior of methylammonium lead iodide planar diodes. Upon biasing the diodes with a positive voltage, the turn-on voltage of the electroluminescence diminishes and its intensity substantially increases. This behavior is reminiscent of that observed in light-emitting electrochemical cells (LECs), single-layer electroluminescent devices in which the charge injection is assisted by the accumulation of ions at the electrode interface. Because of this mechanism, performances are largely independent from the work function of the electrodes. The similarities observed between planar perovskite diodes and LECs suggest that mobile ions in the perovskite do play an important role in device operation. Besides enhanced electroluminescence, biasing these devices can also result in improved photovoltaic performance.

Introduction

In only a few years, organic–inorganic (hybrid) perovskites, such as the archetype compound methylammonium lead iodide ($MAPbI_3$), have become the most promising materials for future photovoltaic applications, following the demonstration of power conversion efficiencies (PCE) exceeding 20%.[1–3] This PCE could be achieved because of the unique combination of characteristics such as high optical absorption,[4] low bandgap,[5] low exciton binding energy (mainly free carriers are present at room temperature),[6,7] and long-range carrier diffusion length.[8] Hybrid perovskites with wider bandgap have been also used in electroluminescent devices, showing promising efficiencies and electroluminescence intensity.[9–12] High-quality hybrid perovskite thin films can be processed by simple solution or sublimation methods, allowing the preparation of simple and potentially inexpensive photovoltaic devices. Despite such important advantages, some issues need to be addressed before perovskite solar cells can be commercialized. Most perovskites are very sensitive to oxygen and moisture and degrade rapidly in ambient conditions; hence, many studies are devoted to mitigating this instability.[13] Another important aspect is that simple current–voltage sweeps in $MAPbI_3$ solar cells are characterized by a certain degree of hysteresis, and slow transient phenomena often affect the measurements.[14] Several mechanisms responsible for the hysteretic behavior of perovskites have been proposed, *i.e.* capacitive effects due to the interaction between the perovskite and charge transport materials,[15] electronic traps at the interface or grain boundaries of the perovskite,[16] the light-activated reorientation of the MA^+ cations under bias,[17] or a mixed electronic–ionic conductivity, which would imply that mobile ions are present in the bulk of perovskites.[18,19] Theoretical calculations predicted iodide to be the most mobile ion in $MAPbI_3$ thin films (due to lower activation energy for ion migration). The actual I^- motion under external bias has been observed through indirect evidence,[20] and recently, deQuilettes *et al.* also demonstrated that iodide migration can take place in perovskite under illumination.[21] Iodine vacancies and interstitial defects, on the other hand, would play a relevant role only on a timescale of nanoseconds, many orders of magnitude shorter than that of a conventional current density–voltage (J–V) scan.[22] Also, recent experimental observations of ionic redistribution within a perovskite active layer under external bias suggested the migrating species to be the methylammonium ion.[23] Independently from their nature, free ions may originate from non-perfect initial stoichiometry or degradation of the active layer, which leads to the presence of defects and vacancies in the film. Decomposition of the perovskite and reversible generation of free ions due to an external electric field have been also demonstrated at the moderate temperature of 330 K;[24] hence, an analogue effect can be expected at RT, perhaps with a slower time constant. While all these phenomena are most likely, to different extents, responsible for the anomalous hysteresis observed in perovskite devices, the general consensus is that mobile ions are indeed present in perovskites and affect

[a]Instituto de Ciencia Molecular, Universidad de Valencia, C/Catedrático J. Beltrán 2, 46980 Paterna, Spain. E-mail: michele.sessolo@uv.es

[b]Faculty of Mathematics and Natural Sciences, University of Groningen, Nijenborgh 4, 9747 AG, Groningen, Netherlands

† Electronic supplementary information (ESI) available. See DOI: 10.1039/c6ta06854e

the device behavior. As an example, an almost-complete switchable photovoltaic behavior in cells with symmetrical electrodes has been demonstrated after biasing the device for a sufficiently long time.[23] In this work, we examine and compare the electrical and electroluminescent characteristics of ambipolar and single-carrier $MAPbI_3$ planar diodes. By means of a combination of direct current (DC) voltage bias and fast *J–V* sweeps, we show that in ambipolar devices with ohmic charge injection, the electronic processes dominate over the ionic contribution, whereas in hole-only devices, both the current injection and electroluminescence have a strong time- and bias-dependent behavior. The ion redistribution promoted by the applied bias seems to favor the electronic carrier injection by a mechanism already identified in light-emitting electrochemical cells (LECs).[25] The beneficial effect of biasing on a degraded solar cell is shown as a proof of concept.

Results and discussion

The reference $MAPbI_3$ solar cell (device A, energy diagram reported in Fig. 1a) was built on glass slides coated with a pre-patterned indium tin oxide (ITO) electrode. The substrate is coated with a thin (50 nm) film of poly(3,4-ethylenedioxythiophene):polystyrene sulfonate (PEDOT:PSS), followed by a 20 nm thick layer of the electron-blocking material poly(*N*,*N*′-bis(4-butylphenyl)-*N*,*N*′-bis(phenyl)benzidine) (polyTPD). The $MAPbI_3$ perovskite films (100 to 350 nm) were deposited by dual-source vapor deposition using previously published protocols.[26] The fullerene derivative indene–C_{60}–propionic acid hexyl ester (IPH) was then deposited on top by spin-coating, thus acting as the electron transport layer (ETL, 50 nm).[27] The device is finished with a barium/silver anode in the case of the ambipolar devices (Fig. 1b). The hole-only device

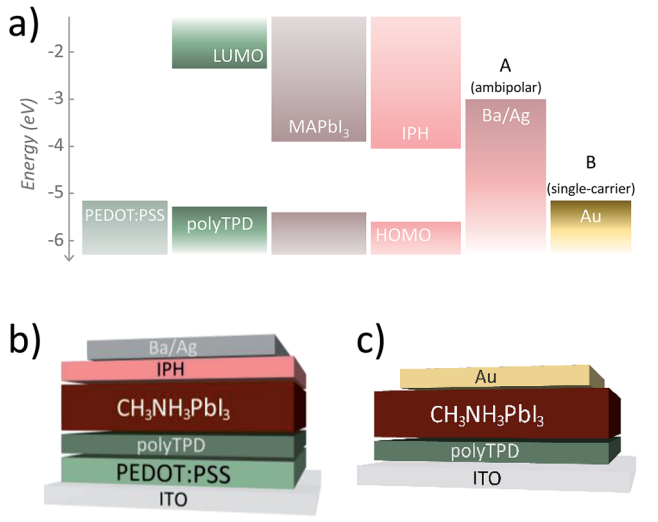

Fig. 1 (a) Flat-band energy diagram for the materials used in device A (Ba/Ag electrode, ambipolar injection) and device B (Au electrode, single-carrier diode). (b) Structure of the reference (ohmic) device with the PEDOT:PSS as the hole injection layer and the Ba/Ag anode. (c) Structure of the single-carrier device, without PEDOT:PSS and with the Au anode.

(device B) does not contain the PEDOT:PSS and IPH layers, and the top electrode is replaced with gold (Fig. 1c). Given the large work function of Au with respect to Ba, a high energy barrier for electron injection is created.

The reference device A, with a $MAPbI_3$ absorber thickness of 350 nm, shows the expected photovoltaic behavior (Fig. S1†), with a high fill factor (80%, Table S1†), negligible hysteresis in the *J–V* scans, and a power conversion efficiency (PCE) of 13.7%. For the biasing experiments, a thinner $MAPbI_3$ absorber was used (100 nm) in order to enhance the effect of the applied field at low bias voltage. The measurements consist of biasing the devices with a constant voltage over time and monitoring the current density evolution. At regular intervals (30 s) during the constant voltage operation, the voltage is changed rapidly ($2\ V\ s^{-1}$), and the resulting current density is measured, leading to *J–V* curves. The fast *J–V* scans allow decoupling of the electronic processes from other slower phenomena affecting the devices. During these *J–V* scans, the minimum sweep voltage V_{sweep} has been kept at 1 V in order to avoid the complete relaxation of the system.[25] All the biasing experiments have been performed in the dark to exclude interferences with photogenerated charge carriers. The near-infrared (NIR) electroluminescence has been measured with a Si photodiode.

The current density and radiant flux *versus* time for device A at various constant bias voltages (V_{bias}) is reported in Fig. 2a and 2b. Below a bias of 1 V, the current density is very small, and no substantial electroluminescence was detected. For $V_{bias} > 1.0$ V, a monotonic increase in the current density can be observed with increasing constant bias voltage (Fig. 2a). At each bias voltage, the current transient is monitored, showing a slow rise and then leveling off towards a plateau. For bias voltages above 3.0 V, a maximum current density is reached, after which the current density decreases, and no plateau is observed. The slow increase in current density (bias voltage dependent) is due to a decrease of the charge injection barrier, or an increase in the layer conductivity *versus* time, or to both these effects. The timescale of the current increase is similar to what has been observed in LECs, where ion migration has been identified as the origin of this effect.[25,28,29] The electroluminescence evolution was simultaneously monitored for the different voltages applied (Fig. 2b). The diodes that were biased at voltages above 1.5 V showed a strong decrease of the electroluminescence during the first 30–60 seconds. Such a sudden decrease of the electroluminescence might be due to the formation of quenching species in the proximity of the recombination zone, a consequence of the decomposition of $MAPbI_3$ under the strong electric field ($>9\ V\ \mu m^{-1}$ for $V_{bias} \geq 1.5$ V).[24]

To investigate the observed changes in current density and electroluminescence, fast *J–V* scans ($1.0\ V \leq V_{sweep} \leq 3.5\ V$) were performed after 30 s of biasing for the different V_{bias} values (Fig. 2c–e). With increasing V_{bias}, a small increase in the maximum current density and in the diodes' built-in voltage V_{bi} (estimated as the point where *J* deviates from the exponential dependence with V_{sweep}, ref. 30) is observed (Fig. 2c). The turn-on voltage for light emission is low and remains constant at about 1.0 V independently from V_{bias} (Fig. 2d). Interestingly, for $V_{bias} \geq 2.0$ V we do observe a decrease of the

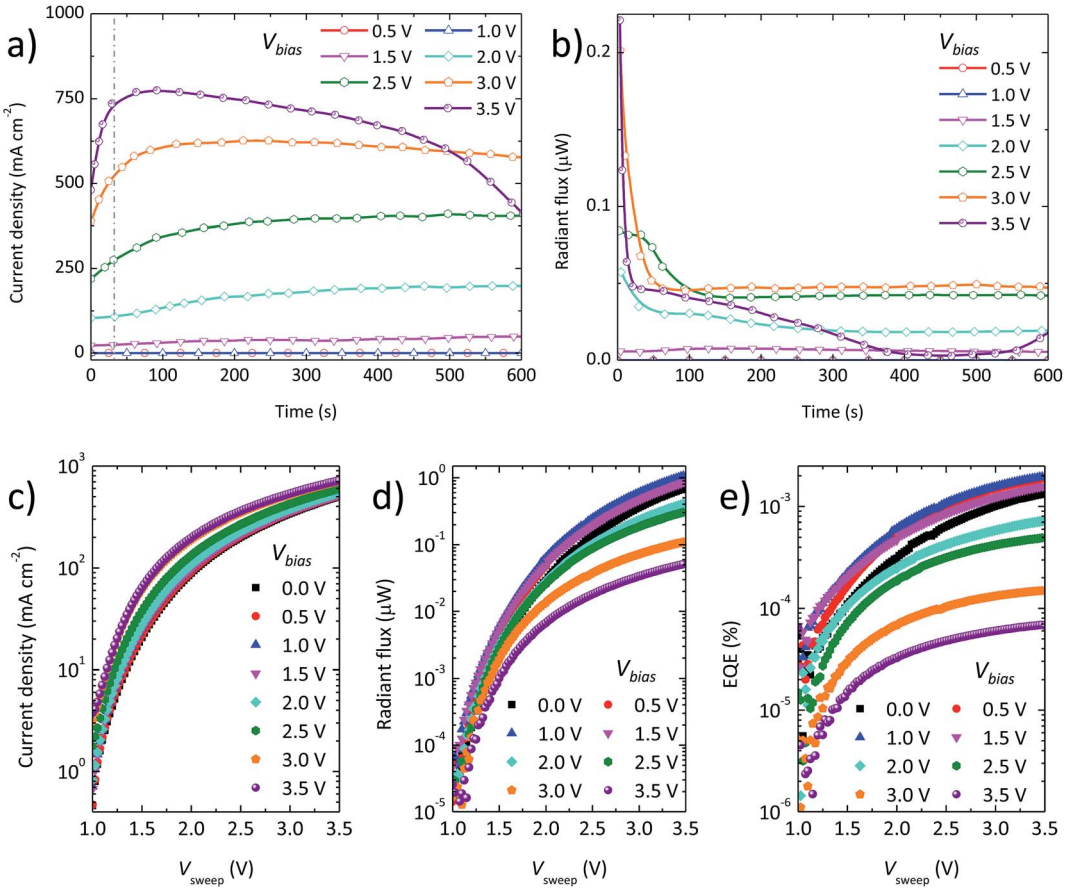

Fig. 2 (a) DC component of the current density and (b) radiant flux *versus* time for the perovskite diode A (ambipolar) for increasing voltage (V_{bias}). (c) Current density, (d) radiant flux and (e) external quantum efficiency (EQE) *versus* applied voltage during fast scans, (V_{sweep}) measured after 30 s biasing at different constant bias voltages.

electroluminescence intensity. Such a performance decrease is very clearly observed from the trend of the external quantum efficiency for electroluminescence *versus* V_{bias} (EQE, Fig. 2e). The increased current density and the simultaneous decrease in electroluminescence at large V_{bias} may be due to the formation of regions with a high density of charge carriers adjacent to the electrode interfaces. At the same time, migration of ions promoted by relatively high values of voltage bias can introduce vacancy defects in the perovskite framework, which can act as traps, giving place to non-radiative recombination for the electrons and holes. In the type A devices, due to the presence of energetically matched electrodes and charge transport materials (Fig. 1), virtually no injection barriers are present. Hence, the ionic effects within the perovskite layer are largely masked by the high current density passing through the device. Also, the slight increase in the current density might be attributed to the interaction between I^- anions and the fullerene acceptor IPH, as recently reported.[20] For the above reasons and to put in evidence the role of the ionic charges in $MAPbI_3$, we prepared single-carrier devices (device B) by replacing the IPH/Ba–Ag with a bare Au electrode and by removing the PEDOT:PSS film. The PEDOT:PSS layer was removed to avoid any transient contribution from the PSS polyelectrolyte.

As expected from the energy level alignment of device B, the current density measured over time for different V_{bias} (Fig. 3a) is much lower with respect to type A devices, and no electroluminescence could be detected in the voltage range used. In type B devices, we observed degradation for $V_{bias} > 1.5$ V, as can be seen by the fast rise and drop of the current density when the device is biased constantly at $V_{bias} = 1.75$ V. Due to the large energy barrier at the $MAPbI_3$/Au interface, the applied bias is likely to drop almost entirely at this interface, causing degradation of the perovskite and hence a drastic decrease of the current density. Also for the single-carrier devices, a slow component in the transient current density is present in the first 50 s of the measurement, suggesting that similar processes are occurring for both types of devices (A and B). Hence, we analyzed the fast *J*–*V* scans obtained for $V_{bias} \leq 1.5$ V after biasing the device for 30 s. For moderate forward-constant biases ($V_{bias} \leq 0.5$ V), the current density is low and does not show the expected exponential increase as for the diode A (Fig. 3b). In the same voltage range, only very weak electroluminescence is detected, with turn-on voltages as high as 3.0 V (Fig. 3c). With increasing applied constant bias ($V_{bias} > 0.75$ V), however, the slope of the fast *J*–*V* scan becomes steeper, and for $V_{bias} \geq 1.0$ V, the current density behavior becomes essentially

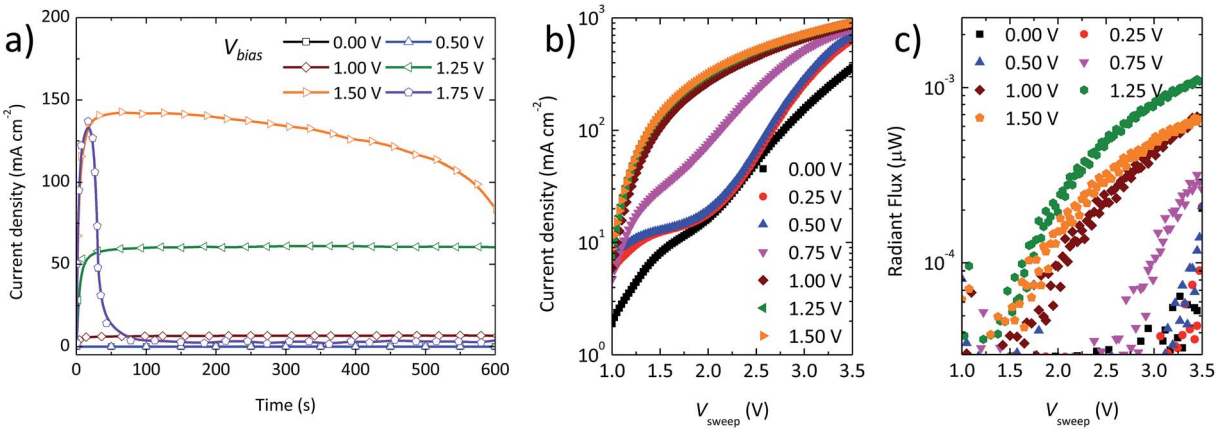

Fig. 3 (a) DC component of the current density for the perovskite diode B (single-carrier device) for increasing constant driving voltage (V_{bias}). (b) Current density and (c) radiant flux *versus* applied voltage during fast scans (V_{sweep}) measured after 30 s bias at different voltages.

analogous to that observed for the ambipolar device (Fig. 2c). Importantly, the radiant flux also increases, and the turn-on voltage gradually shifts towards 1.2 V (Fig. 3c). This, therefore, indicates that the charge carrier injection becomes ambipolar and the injection efficiency is strongly enhanced, as a consequence of positively biasing the device.

In device B, due to a favorable band alignment throughout the ITO/polyTPD/$MAPbI_3$ layers, holes are more efficiently injected than electrons into the perovskite, and the recombination zone is likely to be closer to the perovskite/gold interface, where non-radiative recombination can occur. Biasing device B for a longer time (~300 s) shows no substantial changes in the current density. Nevertheless, electroluminescence can be detected even for $V_{bias} = 0$ V (Fig. S2†), meaning that the processes assisting electron injection take place even under a very low electric field opposing the built-in potential. It is worth mentioning how the current density before and after the fast *J–V* sweep is essentially equal (Fig. S4†), meaning that the energetics at the interfaces (*i.e.* the ionic distribution) is maintained for short times even when the system is driven out of equilibrium.

From the results presented so far, it is evident that forward-biasing the perovskite diodes leads to an improvement in the charge transport in injection-limited devices. As the time scale of the observed phenomena (30–300 s) is compatible with the expected migration rate of the mobile ions in perovskite,[22] and since no other ionic materials can influence the transient behavior observed for device B, the mechanism underlying the incremented performance is similar to the working principle of LECs. These simple luminescent devices consist of a single electroluminescent layer, either an ionic transition metal complex or an electroluminescent polymer added with ionic species, sandwiched between two electrodes.[31,32] When driven in DC, mobile ions in the bulk of the electroluminescent material accumulate towards the interfaces with the electrodes, forming ionic double layers that facilitate the injection of charge carriers, independently of the work function of the electrodes.

Initially, two modes of operation had been proposed for LECs: the electrochemical model (ECM), in which the charge injection is facilitated by the p- and n-doping of the material near the electrodes,[33–36] and the electrodynamic model (EDM), in which the accumulation of ions lowers the barrier for the charge injection without involving any kind of electrochemical doping.[37,38] Nonetheless, these models seem to be the two extremes of one single mixed mechanism that leans towards EDM or ECM depending on the injection-limited or non-injection-limited character of the device, respectively.[29] Independently of the preferential injection and transport process, the charges in a LEC recombine in the bulk of the emissive layer to give light. The same mechanism is able to explain the behavior of our perovskite diodes. As shown in Fig. 4a, in open-circuit conditions, the ions of opposite signs are uniformly distributed within the active layer. When a constant bias is applied, the ions redistribute, drifting towards the respective electrodes. The ionic accumulation at the perovskite/metal interface is able to assist the electron injection even in a single-carrier device,

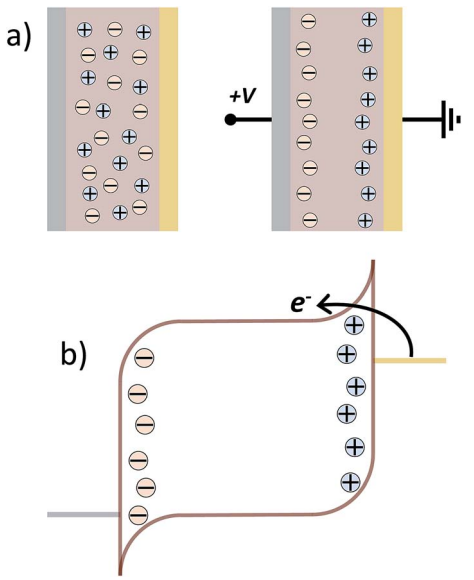

Fig. 4 (a) Schematics of the ionic redistribution following the application of an external bias within a planar diode and (b) simplified energy diagram of the single-carrier device B after biasing.

leading to electroluminescence after biasing. While the injection for holes is nearly ohmic, electrons can tunnel through the injection barrier when enough ions are accumulated at the interface (Fig. 4b). Therefore, the recombination zone is shifted towards the gold cathode, where quenching due to the presence of the metal or due to high ion density reduces the electroluminescence with respect to a device of type A, in which the recombination is expected to take place closer to the center of the perovskite layer. Whether the easier electron injection under bias is due to the lowering of the injection barrier or to an electrochemical doping process is still unknown, but, as we will see in the following, the decrease of the photocurrent for a solar cell under bias may indicate that to some extent, electrochemical doping takes place. It is interesting to note that the turn-on of DC voltage-driven LECs with a comparable thickness of the active layer ~100 nm can be very slow, from many minutes to hours in their simplest configuration,[39] and in any case, it needs electric fields of about 30 V μm^{-1} even for the faster LECs.[40] In the case of hybrid perovskites, this process appears to be much faster, and the fields needed to actually displace the ions from equilibrium can be <4.5 V μm^{-1} (device B, with an inter-electrode spacing of 115 nm, shows light emission after 30 s at 0.5 V bias). Some reports for the analogue bromide perovskite $CH_3NH_3PbBr_3$ suggest that ion migration can be triggered by fields as low as 0.5 V μm^{-1}.[41]

Vacuum-deposited perovskite films, as those used in this work, are composed by densely packed grains with size of about 100–200 nm,[42] which is on the same order of magnitude of the thickness of the films used here (100 nm). In these conditions, ion migration can take place through the grain, as well as through highly defective zones such as grain boundaries.[43] Independently of the actual ionic channel, ions can locally drift, accumulating or depleting at the interfaces between the perovskite emitter and the charge transport materials (modulating the interfacial charge transfer), leaving the light-emitting zone unaffected. In order to see whether the bias-dependent behavior can be applied to improve injection-limited devices, a degraded, air-exposed perovskite solar cell with strong s-shaped *J–V* characteristic was used. Such aged cell initially showed an open-circuit voltage (V_{oc}) of 957 mV, a short-circuit current (J_{sc}) of 11.53 mA cm^{-2} and a poor fill factor (FF) of 28.53%, resulting in a power conversion efficiency (PCE) of 3.15%. As can be seen in Fig. 5a, the unbiased device shows a marked s-shape around V_{oc} associated with hindered charge extraction and causing the low FF. The s-shaped feature is present when the maximum V_{oc} of a solar cell is higher than the built-in voltage V_{bi}.[44] Interestingly, the positive biasing of the perovskite diode actually improves the charge extraction and eliminates the s-shaped feature. This phenomenon can be understood by taking into account the reduction of the energy difference between the perovskite and ETL LUMO levels associated with forward-biasing the device (as observed by measuring the electroluminescence). This, in turn, recovers the device V_{bi} and hence the solar cell FF (Fig. S5†). After 300 s biasing in the dark at voltages ranging from 0.0 V to 2.5 V, the s-shape gradually disappears and the FF steadily increases (Fig. 5b). Even if the s-shape completely vanishes only at 2.0 V, the maximum gain in efficiency is reached at a bias of 1.5 V because of a decrease of the current density. The decrease of the current density can be explained again considering the accepted working mechanism of LECs, where ion redistribution under the applied field leaves an intrinsic zone in the middle of the active layer, hence reducing the effective thickness of the perovskite absorber. As anticipated, this may be an indication of the formation of electrochemical doped zones acting as quenchers for the electroluminescence. The thickness of the intrinsic (undoped) zone can be estimated by the linear relation between the photocurrent and the effective thickness of the absorbing layer: the initial 11.53 mA cm^{-2} photocurrent for the device without applied bias (100 nm perovskite thickness) decreases to 7.69 mA cm^{-2} after 300 s biasing in the dark at 2.5 V. This leads to a value of ~67 nm for the thickness of the intrinsic zone, where charge carriers are photo-generated. This is in agreement with the value reported by Meier *et al.* for the thickness of the undoped zone in ionic transition metal complex-based LECs (iTMC-LECs) at steady state (around 60% of the total active layer).[45] In general, the efficiency of the degraded device increases in the range of 1.5–2.0 V applied bias, reaching a maximum value of 4.87%, more than a 50% relative increase (Fig. 5c).

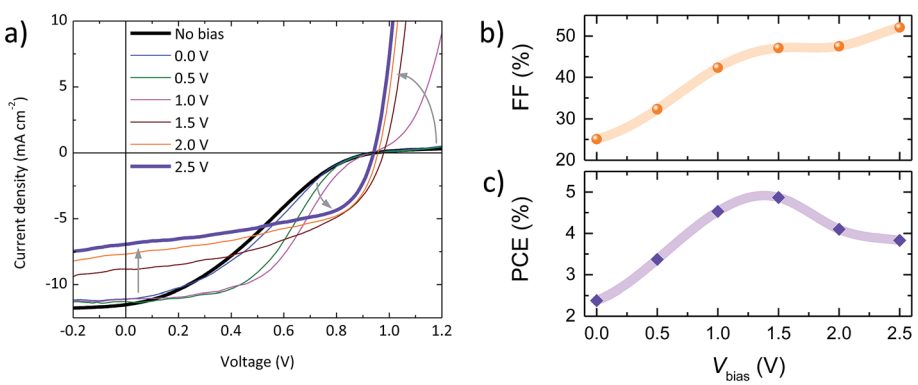

Fig. 5 (a) Evolution of the *J–V* characteristics with increasing applied voltages (V_{bias}) for a degraded solar cell biased in the dark (thick black line refers to the pristine device, the thick purple line to the device after biasing at 2.5 V for 300 s). (b) Trend of the fill factor and of the (c) PCE extracted from the same curves.

Conclusions

By means of a combination of forward-DC biasing and fast *J–V* scans, we have demonstrated that it is possible to enhance the charge injection into the bulk of perovskite diodes. A device with misaligned energy levels behaves under DC bias as a light-emitting electrochemical cell, suggesting the presence of free ions in the perovskite, which are able to assist the current injection. This is confirmed by monitoring the electroluminescence of single-carrier devices, which gradually appears with lower turn-on voltages and increasing biasing voltage and time.

We show that a degraded solar cell can be partially recovered upon biasing in the dark. The relative efficiency gain is over 50%, mainly due to the increased FF, *i.e.* to the better charge extraction. The decrease of the photocurrent for the same device points toward an electrochemical doping mechanism similar to that already observed in LECs, in which it is responsible for the enhanced charge injection and extraction.

Experimental section

Device fabrication

ITO-covered glass substrates were purchased from Naranjo Substrates. Poly(3,4-ethylenedioxythiophene):poly(styrenesulfonic acid) (PEDOT:PSS) CLEVIOS P VP AI 4083 was purchased from Hereaus Holding and used as received. Poly[*N*,*N*′-bis(4-butylphenyl)-*N*,*N*′-bis(phenyl)benzidine (polyTPD) was purchased from American Dye Source. Indene–C_{60}–propionic acid hexyl ester (IPH) was purchased from Solenne B.V. For their application, polyTPD and IPH were dissolved in chlorobenzene at 7 mg mL^{-1} and 20 mg mL^{-1}, respectively. PbI_2 was purchased from TCI, and CH_3NH_3I from Lumtec; both were used as received.

Devices were prepared on cleaned ITO substrates by spin-coating a thin layer (70 nm) of PEDOT:PSS. On top of this, a thin film of polyTPD (20 nm) was deposited from its chlorobenzene solution. The perovskite was synthesized using a vacuum chamber (1×10^{-6} mbar) integrated in an MBraun glovebox filled with inert gas N_2. The starting materials, CH_3NH_3I and PbI_2, were placed in ceramic crucibles and heated up to 70 °C and 250 °C, respectively. The perovskite layer was then thermally evaporated using a protocol described previously.[26] The IPH layer (40 nm) was deposited from its chlorobenzene solution by spin coating. The metal electrode Ba was thermally evaporated under a base pressure of 2×10^{-6} mbar to a thickness of 10 nm. The devices were then finished by evaporating a 100 nm Ag layer immediately after the Ba.

Device characterization

Diode characterization was performed using a mini sun simulator with a halogen lamp designed by ECN and calibrated with a Si reference cell. The non-encapsulated solar cells were measured in a N_2-filled glovebox. The current density (*J*) *versus* voltage (*V*) characteristics were measured in the dark and under illumination using a 10^{-2} cm^2 shadow mask to prohibit lateral current collection from outside the active area. The bias-sweep experiments were performed on fresh, non-encapsulated devices in a glovebox filled with N_2. A Keithley 2636B Voltage Meter unit, driven by a custom-made LabView program, was used as the voltage source and for the measurement of the current-*versus*-voltage and photocurrent-*versus*-voltage characteristics. The photocurrent was measured directly as the response to the IR emission from a Hamamatsu Si photodiode. The experiments on the aged cell were performed in air on unencapsulated samples kept for a week in air. The tests were performed using a solar simulator calibrated with a Si solar cell. The biasing of the perovskite diodes was performed in the dark, while the *J–V* curves were measured under AM 1.5 illumination on a Keithley 2636B Voltage Meter unit using a custom-made LabView program. A shadow mask with an aperture of 10^{-2} cm^2 was used to limit the illuminated area to the central part of the device.

Acknowledgements

We acknowledge financial support from the European Union H2020 project INFORM (grant 675867), the Spanish Ministry of Economy and Competitiveness (MINECO) *via* the Unidad de Excelencia María de Maeztu MDM-2015-0538, MAT2014-55200 and PCIN-2015-255, and the Generalitat Valenciana (Prometeo/2012/053). M. S. and E. B. thank the MINECO for their post-doctoral (JdC) and pre-doctoral grants, respectively. J. A. thanks the Spanish Ministry of Education, Culture and Sport for his pre-doctoral grant.

Notes and references

1 W. S. Yang, J. H. Noh, N. J. Jeon, Y. C. Kim, S. Ryu, J. Seo and S. I. Seok, *Science*, 2015, **348**, 1234–1237.
2 M. Saliba, T. Matsui, J.-Y. Seo, K. Domanski, J.-P. Correa-Baena, M. K. Nazeeruddin, S. M. Zakeeruddin, W. Tress, A. Abate, A. Hagfeldt and M. Grätzel, *Energy Environ. Sci.*, 2016, **9**, 1989–1997.
3 Y. Zhao, J. Wei, H. Li, Y. Yan, W. Zhou, D. Yu and Q. Zhao, *Nat. Commun.*, 2016, **7**, 10228.
4 W. J. Yin, T. Shi and Y. Yan, *Adv. Mater.*, 2014, **26**, 4653–4658.
5 M. M. Lee, J. Teuscher, T. Miyasaka, T. N. Murakami and H. J. Snaith, *Science*, 2012, **338**, 643–647.
6 A. Miyata, A. Mitioglu, P. Plochocka, O. Portugall, J. T.-W. Wang, S. D. Stranks, H. J. Snaith and R. J. Nicholas, *Nat. Phys.*, 2015, **11**, 582–587.
7 K. Galkowski, A. Mitioglu, A. Miyata, P. Plochocka, O. Portugall, G. E. Eperon, J. T.-W. Wang, T. Stergiopoulos, S. D. Stranks, H. J. Snaith and R. J. Nicholas, *Energy Environ. Sci.*, 2016, **9**, 962–970.
8 S. D. Stranks, G. E. Eperon, G. Grancini, C. Menelaou, M. J. Alcocer, T. Leijtens, L. M. Herz, A. Petrozza and H. J. Snaith, *Science*, 2013, **342**, 341–344.
9 Y. H. Kim, H. Cho, J. H. Heo, T. S. Kim, N. Myoung, C. L. Lee, S. H. Im and T. W. Lee, *Adv. Mater.*, 2015, **27**, 1248–1254.
10 H. Cho, S. H. Jeong, M. H. Park, Y. H. Kim, C. Wolf, C. L. Lee, J. H. Heo, A. Sadhanala, N. Myoung, S. Yoo, S. H. Im, R. H. Friend and T. W. Lee, *Science*, 2015, **350**, 1222–1225.

11 M. Sessolo, L. Gil-Escrig, G. Longo and H. J. Bolink, *Top. Curr. Chem.*, 2016, **374**, 52.
12 Y.-H. Kim, H. Cho and T.-W. Lee, *Proc. Natl. Acad. Sci. U. S. A.*, 2016, **113**, 11694–11702.
13 J. S. Manser, M. I. Saidaminov, J. A. Christians, O. M. Bakr and P. V. Kamat, *Acc. Chem. Res.*, 2016, **49**, 330–338.
14 E. L. Unger, E. T. Hoke, C. D. Bailie, W. H. Nguyen, A. R. Bowring, T. Heumüller, M. G. Christoforo and M. D. McGehee, *Energy Environ. Sci.*, 2014, **7**, 3690–3698.
15 H. S. Kim, I. H. Jang, N. Ahn, M. Choi, A. Guerrero, J. Bisquert and N. G. Park, *J. Phys. Chem. Lett.*, 2015, **6**, 4633–4639.
16 Y. Shao, Z. Xiao, C. Bi, Y. Yuan and J. Huang, *Nat. Commun.*, 2014, **5**, 5784.
17 R. Gottesman, E. Haltzi, L. Gouda, S. Tirosh, Y. Bouhadana, A. Zaban, E. Mosconi and F. De Angelis, *J. Phys. Chem. Lett.*, 2014, **5**, 2662–2669.
18 H. J. Snaith, A. Abate, J. M. Ball, G. E. Eperon, T. Leijtens, N. K. Noel, S. D. Stranks, J. T. Wang, K. Wojciechowski and W. Zhang, *J. Phys. Chem. Lett.*, 2014, **5**, 1511–1515.
19 J. M. Frost and A. Walsh, *Acc. Chem. Res.*, 2016, **49**, 528–535.
20 M. De Bastiani, G. Dell'Erba, M. Gandini, V. D'Innocenzo, S. Neutzner, A. R. S. Kandada, G. Grancini, M. Binda, M. Prato, J. M. Ball, M. Caironi and A. Petrozza, *Adv. Energy Mater.*, 2016, **6**, 1501453.
21 D. W. deQuilettes, W. Zhang, V. M. Burlakov, D. J. Graham, T. Leijtens, A. Osherov, V. Bulovic, H. J. Snaith, D. S. Ginger and S. D. Stranks, *Nat. Commun.*, 2016, **7**, 11683.
22 J. M. Azpiroz, E. Mosconi, J. Bisquert and F. De Angelis, *Energy Environ. Sci.*, 2015, **8**, 2118–2127.
23 Y. Yuan, J. Chae, Y. Shao, Q. Wang, Z. Xiao, A. Centrone and J. Huang, *Adv. Energy Mater.*, 2015, **5**, 1500615.
24 Y. Yuan, Q. Wang, Y. Shao, H. Lu, T. Li, A. Gruverman and J. Huang, *Adv. Energy Mater.*, 2016, **6**, 1501803.
25 M. Lenes, G. Garcia-Belmonte, D. Tordera, A. Pertegás, J. Bisquert and H. J. Bolink, *Adv. Funct. Mater.*, 2011, **21**, 1581–1586.
26 M. Liu, M. B. Johnston and H. J. Snaith, *Nature*, 2013, **501**, 395–398.
27 L. Gil-Escrig, C. Momblona, M. Sessolo and H. J. Bolink, *J. Mater. Chem. A*, 2016, **4**, 3667–3672.
28 Q. Pei, G. Yu, C. Zhang, Y. Yang and A. J. Heeger, *Science*, 1995, **269**, 1086–1088.
29 S. van Reenen, P. Matyba, A. Dzwilewski, R. A. Janssen, L. Edman and M. Kemerink, *J. Am. Chem. Soc.*, 2010, **132**, 13776–13781.
30 G.-J. A. H. Wetzelaer and P. W. M. Blom, *NPG Asia Mater.*, 2014, **6**, e110.
31 S. Tang and L. Edman, *Top. Curr. Chem.*, 2016, **374**, 40.
32 S. B. Meier, D. Tordera, A. Pertegás, C. Roldán-Carmona, E. Ortí and H. J. Bolink, *Mater. Today*, 2014, **17**, 217–223.
33 J. Gao and J. Dane, *Appl. Phys. Lett.*, 2004, **84**, 2778.
34 D. J. Dick, A. J. Heeger, Y. Yang and Q. Pei, *Adv. Mater.*, 1996, **8**, 985–987.
35 C. V. Hoven, H. Wang, M. Elbing, L. Garner, D. Winkelhaus and G. C. Bazan, *Nat. Mater.*, 2010, **9**, 249–252.
36 P. Matyba, K. Maturova, M. Kemerink, N. D. Robinson and L. Edman, *Nat. Mater.*, 2009, **8**, 672–676.
37 J. C. deMello, N. Tessler, S. C. Graham and R. H. Friend, *Phys. Rev. B: Condens. Matter Mater. Phys.*, 1998, **57**, 12951–12963.
38 G. G. Malliaras, J. D. Slinker, J. A. DeFranco, M. J. Jaquith, W. R. Silveira, Y.-W. Zhong, J. M. Moran-Mirabal, H. G. Craighead, H. D. Abruna and J. A. Marohn, *Nat. Mater.*, 2008, **7**, 168.
39 S. T. Parker, J. D. Slinker, M. S. Lowry, M. P. Cox, S. Bernhard and G. G. Malliaras, *Chem. Mater.*, 2005, **17**, 3187–3190.
40 E. Zysman-Colman, J. D. Slinker, J. B. Parker, G. G. Malliaras and S. Bernhard, *Chem. Mater.*, 2008, **20**, 388–396.
41 S. Chen, X. Wen, R. Sheng, S. Huang, X. Deng, M. A. Green and A. Ho-Baillie, *ACS Appl. Mater. Interfaces*, 2016, **8**, 5351–5357.
42 C. Momblona, L. Gil-Escrig, E. Bandiello, E. M. Hutter, M. Sessolo, K. Lederer, J. Blochwitz-Nimoth and H. J. Bolink, *Energy Environ. Sci.*, 2016, **9**, 3456–3463.
43 Y. Shao, Y. Fang, T. Li, Q. Wang, Q. Dong, Y. Deng, Y. Yuan, H. Wei, M. Wang, A. Gruverman, J. Shield and J. Huang, *Energy Environ. Sci.*, 2016, **9**, 1752–1759.
44 M. Lenes and H. J. Bolink, *ACS Appl. Mater. Interfaces*, 2010, **2**, 3664–3668.
45 S. B. Meier, D. Hartmann, A. Winnacker and W. Sarfert, *J. Appl. Phys.*, 2014, **116**, 104504.

